NOTICE
PORTIONS OF THIS REPORT ARE ILLEGIBLE.
It has been reproduced from the best available copy to permit the broadest possible availability.

CONF-8403148--1

CONF-8403148--1

DE85 001096

X-RAY MICROPROBE CHARACTERIZATION OF MATERIALS: THE CASE FOR UNDULATORS ON ADVANCED STORAGE RINGS*

C. J. Sparks, Jr.
Metals and Ceramics Division
Oak Ridge National Laboratory
Oak Ridge, Tennessee 37831

MASTER

Presentation to the

MAJOR MATERIALS FACILITIES COMMITTEE
NATIONAL RESEARCH COUNCIL
Washington, D.C.

March 17, 1984

DISCLAIMER

This report was prepared as an account of work sponsored by an agency of the United States Government. Neither the United States Government nor any agency thereof, nor any of their employees, makes any warranty, express or implied, or assumes any legal liability or responsibility for the accuracy, completeness, or usefulness of any information, apparatus, product, or process disclosed, or represents that its use would not infringe privately owned rights. Reference herein to any specific commercial product, process, or service by trade name, trademark, manufacturer, or otherwise does not necessarily constitute or imply its endorsement, recommendation, or favoring by the United States Government or any agency thereof. The views and opinions of authors expressed herein do not necessarily state or reflect those of the United States Government or any agency thereof.

*Research sponsored by the Division of Materials Sciences, U.S. Department of Energy under contract DE-AC05-84OR21400 with the Martin Marietta Energy Systems, Inc.

By acceptance of this article, the publisher or recipient acknowledges the U.S. Government's right to retain a nonexclusive, royalty-free license in and to any copyright covering the article.

DISTRIBUTION OF THIS DOCUMENT IS UNLIMITED

X-ray microprobe characterization of materials: the case for undulators on advanced storage rings

C. J. Sparks, Jr.
Oak Ridge National Laboratory, P. O. Box X, Oak Ridge, Tennessee 37831

ABSTRACT

The unique properties of X rays offer many advantages over electrons and other charged particles for the microcharacterization of materials. X rays are more efficient in exciting characteristic X-ray fluorescence and produce higher fluorescent signals to backgrounds than obtained with electrons. Detectable limits for X rays are a few parts per billion and are 10^{-3} to 10^{-5} less than for electrons. Energy deposition in the sample by X rays is 10^{-3} to 10^{-4} less than for electrons for the same detectable concentration. High-brightness storage rings, especially in the 6 GeV class with undulators, will be approximately 10^3 brighter in the X-ray energy range from 5 keV to 35 keV than existing storage rings and provide for X-ray microprobes that are as bright as the most advanced electron probes. Such X-ray microprobes will produce unprecedented low levels of detection in diffraction, EXAFS, Auger, and photoelectron spectroscopies for both chemical characterization and elemental identification. These major improvements in microcharacterization capabilities will have wide-ranging ramifications not only in materials science but also in physics, chemistry, geochemistry, biology, and medicine.

I. INTRODUCTION

Efforts to obtain micro-diffraction and micro-elemental analysis to understand the properties of matter have been made since the early part of this century when the first X-ray probes were constructed. Conferences have been held on the design and application of X-ray microprobe sources.[1] In the early 1950s there was an upsurge in interest in microanalytical methods. Microprobes with electrons to bombard the sample quickly become the instrument of choice for microcharacterization. Electrons could easily be focused to spot sizes less than 1 µm-diam with enormous intensities compared to X-ray sources. Though X-ray excitations give a much better signal to background, their generation required electron bombardment of a metal target with X rays emitted into 4π srad which then had to be gathered and focused to a small spot with inefficient X-ray optics. With the commercial availability of high-intensity and high-resolution electron microprobes, the unique properties of photons could not overcome the lack of intensity from their weak sources. Interest in X rays as an excitation source for microprobe analysis faded, leaving electrons as the dominant microprobe source. It is a conservative estimate that 1200 to 2500 electron probes currently are being used for microcharacterization of matter in the United States. This represents an investment of $1 billion or more in instrumentation alone. The wide usage of analytical microprobes is well documented in

the several yearly conferences and journals of the electron microscopy and microprobe societies and attests to the great emphasis being placed by the scientific community on the need for microstructural characterization of matter.

With the advent of electron storage rings, an intense source of X rays has become available. The energy spectrum in the hard X-ray region is 10^4 to 10^5 times more brilliant than our conventional X-ray sources (2 kw to 60 kw dissipated by electrons impinging on metal targets). In fact, with magnetic devices especially suited for extracting the radiation from proposed new high-brightness storage rings, the brightness in units of photons or particles s^{-1} mm^{-2} $mrad^{-2}$ is 2×10^{19} and equivalent to that for the most advanced electron probes having field-emission electron guns.[2] To achieve this brightness for the energy range from 2 keV to 35 keV requires undulators on low-emittance electron storage rings in the 6 GeV energy range. This energy range covers the electron energy levels of the K- and/or L-shells for all the atoms and is most useful for fluorescent and diffraction analysis. Present X-ray storage rings (NSLS at Brookhaven; SPEAR at SSRL, Stanford; CESAR at CHESS, Cornell) are 10^{-3} to 10^{-4} less bright in this energy range.

The improved brightness of a 6 GeV ring with undulators offers major advantages over present storage rings. Scientists will be able to study the chemical composition, geometrical arrangements of the atoms, and electronic structure at unprecedented low levels of concentration. The chemical identity of the elemental composition of matter is a prerequisite to their synthesis, and knowledge of the geometrical arrangement and chemical bonding of the atoms is fundamental to understanding the basic physical and chemical behavior of materials. Much of our progress in the design of materials has come by trial and error. But the science of materials has advanced rapidly in recent years and microcharacterization techniques have made a major contribution providing both chemical identity and geometrical information about the atoms. Yet modern technology is making increasing demands on materials for better performance in terms of their electrical characteristics and under the most adverse environments of high temperature, corrosive atmosphere, and intense radiation fields. More stringent requirements are being placed on the control of manufacturing methods including tightening restrictions on impurity levels, on structure and compositional variations, on presence of minor phases, and on controlling interfaces.[3-5] The behavior of grain boundaries and other interfaces can determine if a material is ductile and has toughness or is brittle and unreliable for use in structural applications. Minor amounts of second phases can improve the strength of materials or make them unfit for service. Segregation of trace elements to interfaces and second phases can have dramatic effects on the properties of materials. Synergestic effects among trace elements is observed but poorly understood. Concentrations are often below present detectable limits for nondestructive analysis and improved microcharacterization methods are needed. The construction of X-ray microprobes on new high-brightness storage rings will produce unique microcharacterization capabilities unmatched by any other method.

As electron microprobes have clearly dominated the field of microcharacterization, the merits of the use of X rays for excitation of the sample will be compared to electrons. A few of the many possible applications are cited where

microcharacterization is important to advancing our understanding of materials properties. For more extensive information the reader should refer to the electron microscopy and microprobe literature.

II. DETECTION LIMITS WITH X RAYS VERSUS ELECTRONS

A standard definition of the minimum detectable mass fraction[6] based on Poisson counting statistics for 95% confidence in detection is

$$\text{Minimum Detectable Mass Fraction (MDMF)} = 3.29\, C_Z (N_b)^{1/2}/N_S \,, \quad (1)$$

where C_Z is the mass fraction of element Z, N_b the background counts, and N_S the counts in the signal. To evaluate Eq. (1), we need to know the fluorescent cross sections to calculate the number of events in the signal and to evaluate the background. An extensive literature review on this subject provides the information for the evaluation.[7] The relevant data are presented in Figs. 1–3. As shown in Figs. 1 and 2, the number of characteristic fluorescent events is typically 10 to 200 times larger for X-ray excitation than for the same number of electrons. As shown in Fig. 3, the fluorescent signal to background is approximately 10^4 times larger for X-ray excitation than for electron excitation. This extremely favorable property of X rays derives from the fact that about 90% or more of the incident X-ray energy is dissipated by ionization of the inner shells. In contrast, only 0.1% of the energy dissipated by electrons gives rise to the fluorescent radiation of interest. Much of their energy is consumed by interactions with the least-bound outer-shell electrons. The deceleration of the incident electrons in the target produces Bremsstrahlung radiation which is responsible for most of the background beneath the fluorescent signals of interest.

We find that 10^{-3} fewer X rays than electrons are required for the same MDMF. In terms of energy deposited, electron energies from 20 keV to 100 keV usually exceed by three to ten times the ionization energy of the bound electron. X-ray energies can be chosen to lie just above the ionization energy (2 keV to 33 keV). As 10^3 more electrons with energies from three to ten times those of X rays are required for the same MDMF, the energy deposited by electrons is 3×10^3 to 10^4 times that deposited by X rays in thick targets. For thin targets most of the incident electron energy is transmitted, but even less incident X-ray energy is absorbed. In air-dried blood cells and 8 μm-thick tissue sections[8] exposed to synchrotron radiation and charged particles, X-ray fluences 10^2 to 10^3 times greater were required to produce similar damage. X-radiation damage to the samples may be orders of magnitude less than the comparison made on the basis of energy deposition alone. Thus with X-ray excitation we have the important choice of being able to either lower the detectable limits for the same fluences or to reduce the radiation damage and heat deposited in the sample for the same MDMF. Since heating and radiation damage of organic samples is of primary concern in modern electron probes, X rays offer major improvements.

III. X-RAY INTENSITIES FROM UNDULATORS ON HIGH-BRIGHTNESS STORAGE RINGS

With the proposed X-ray intensities from undulators on high-brightness storage rings (see other sections of this document and SSRL Report 83/01 and NSLS Report, Planned Evolution of NSLS, October 1983), fluxes are predicted to be on the order of 2.7×10^{15} X rays s^{-1} in an energy bandwidth, $\Delta E/E$, of 0.1%. Projections of an electron source size in the storage ring of $2\sigma_x = 0.8$ mm and $2\sigma_y = 0.2$ mm and divergences of 0.01 mrad in both the horizontal and vertical planes for undulators produce a brightness of 2×10^{19} X rays s^{-1} mm^{-2} $mrad^{-2}$. Considerations of the X-ray-focusing optics[7,9,10] have shown that demagnifications of 100:1 are clearly feasible with about 50% reflection efficiencies and that demagnifications approaching 1000:1 may become possible. Because of the small divergence of undulator radiation, X-ray optics can intercept the entire emittance and both focus and monochromate with high efficiency. We base our arguments for the intensities obtainable for an X-ray microprobe on a modest demagnification of 100:1. A demagnification of 100:1 results in a probe size of 2×8 μm^2, and further reduction is achieved by pinholes in heavy metal foils. The predicted intensities are given in Table I. Comparisons are made with those from the brightest storage ring now in commissioning and the most intense electron microprobe sources. A gain of 1.4×10^4 in intensity per eV is obtained over present low-emittance rings. In addition, undulators in comparison to superconducting wigglers peak the energy in narrow bandwidths reducing the heat load on X-ray optics. At 10 eV energy bandwidths the brightness from undulators will match that available from the most advanced electron probes. Though undulators peak the intensity at harmonic energy intervals, energies ranging from 2 keV to 40 keV are available in either the first or second harmonic. When only discrete X-ray energies are selectable from undulators, then 2, 4, 10, 18, and 35 keV or similar energies are acceptable for most microprobes fluorescent and diffraction analysis.[7] For fluorescent excitation, energy spreads of $\Delta E/E = 1$ are acceptable.[7] For diffraction analysis of the compounds present, a $\Delta E/E = 10^{-2}$ to 10^{-3} is required. For microprobe EXAFS analysis and photoelectron spectroscopy, $\Delta E/E$ should be 10^{-4} to 10^{-5}. These energy resolutions can be achieved with presently available nearly perfect crystals, and the microprobe energy resolution tailored to meet the experimental needs of a variety of applications.

IV. SPATIAL RESOLUTION

Inherently, X-ray excitation for microprobe analysis offers the highest spatial resolution in thick samples of any radiation because the low-scattering cross sections of X rays limit the lateral spreading of the probe. Though electron field-emission sources are much smaller (approaching 10 Å-diam) and are focused to diameters of atomic dimensions, lateral spreading of the electrons in matter produce interaction regions of about 1 μm-diam in thick samples.[11] Electron-probe analysis of ferrous materials having specimen thicknesses of 1000 Å to 2000 Å produce an interaction region of approximately 500 Å-diam even though the incident probe diameter is much less. Diffraction limits may keep the useful X-ray probe diameter to 500 Å and greater.[10] An X-ray microprobe with a beam diameter of 500 Å to 1 μm would compete favorably with the spatial resolution of electron microprobes in a great majority of the samples of

interest. For extremely thin particles and films (< 1000 Å), the electron microprobe has spacial resolutions ranging from a few angstrom to a few hundred angstroms. Although 500 Å-diam appears feasible for an X-ray microprobe, it is not a fundamental limit. In a 500 Å-diam probe, the diffraction-limited divergence angle is 5 mrad for 12 keV X rays but only 0.2 mrad for 100 keV electrons. This places a limit of 10 μm to the depth of beam penetration in the sample before divergence of the X-ray beam in the sample exceeds the intended probe size.

V. DETECTION LIMITS FOR AN X-RAY MICROPROBE BASED ON A 6 GeV RING WITH UNDULATORS

A. Fluorescent Elemental Analysis

The minimum detectable mass fraction is calculated with Eq. (1) using the X-ray intensities given in Table I, the fluorescent cross section and yields of Figs. 1 and 2, and the signal to backgrounds from Fig. 3. We assume an analyzing crystal intercepting 1 cm^2 of fluorescent radiation 10 cm from the sample for a solid angle of 10^{-3}. The number of fluorescent counts in the signal is:

$$\frac{\text{Signal Counts (Ns)}}{\text{Sec } 10^{-6}\ \text{gg}^{-1}} = 0.1\ (\text{Thick-target yield}) \times 10^{14} \left(\frac{\text{Incident Photons}}{\text{Sec } \mu\text{m}^2}\right)$$

$$\times\ 10^{-3}(\text{Solid Angle}) \times 10^{-6}\ (\text{Mass Fraction of } 10^{-6}\ \text{gg}^{-1}):$$

$$\frac{N_s}{\text{Sec } 10^{-6}\text{gg}^{-1}} = 10^4 \frac{\text{Counts}}{\text{Sec } 10^{-6}\text{gg}^{-1}} \text{ from a 1 } \mu\text{m}^2 \text{ spot.}$$

With a signal to background of 10:1 at 10^{-6} gg^{-1} and a homogeneous distribution of the element, the MDMF is 10.5×10^{-9} gg^{-1} s^{-1} which is 2×10^{-4} times the MDMF for the best electron probes with wavelength dispersive optics. An increase to 100 secs counting time would lower the MDMF to 1.5×10^{-9} gg^{-1}.

As the detection of elements at interfaces is important to many materials problems, we calculate the detectable levels for a planer distribution of elements. Assume that one monolayer of an impurity element replaces one 2 Å-wide atomic plane. For an X-ray probe diameter of 1 μm^2, 5000 atomic planes end-on would be irradiated by the beam. Since one of the atomic planes out of 5000 consists of impurity atoms, the concentration of the impurity is 2×10^{-4} gg^{-1} in the volume irradiated by the probe. (This assumes that none of the impurity exists outside the boundary.) Since the MDMF is 10.5×10^{-9} gg^{-1} s^{-1}, then the detection of 5×10^{-5} of a monolayer s^{-1} of impurity is feasible. However, in

most materials we expect some of the impurity to be distributed in the matrix. Typical elemental concentrations of 2×10^{-3} to 10^{-4} gg^{-1} are used to affect grain-boundary behavior. Plotted in Fig. 4 are the calculated profiles of X-ray-probe scans for an iron sample containing 0.1 wt % titanium uniformly distributed in the matrix and with one monolayer of titanium in the grain boundary. The shape and size of the microprobe beam can be defined by pinhole apertures to better match the geometry of the interface to improve the contrast and lower the detectable limit. For this case of titanium in iron where 0.1 wt % of the same impurity is in the matrix, the minimum detectable impurity with the plane of the grain boundary parallel to the direction of the probe (end on) is 5×10^{-3} of a monolayer for both the 1 μm^2 and 500 $Å^2$ probes. As predicted by Eq. (1) a decrease in the probe diameter does not change the detectable limits for a line distribution since the signal decreases linearly and the background decreases as the square of the probe size. If the region next to the boundary is denuded of the impurity, then the smaller probe size has the advantage of better providing the spatial resolution to determine that information. The rectangular-shaped probe has a detectable limit of 6×10^{-4} of a monolayer in the presence of 0.1 wt % in the matrix. Typical experience with advanced analytical electron probes is that one monolayer of impurity at a boundary is at the detection limit.

For impurity atoms and particles or second phases on surfaces and exposed interfaces the characteristic fluorescence or diffracted radiation is not absorbed by the matrix and even lower detection limits are possible. The number of signal counts is

$$\frac{N_S \text{ (Signal counts)}}{\text{Sec atom}} = \frac{I_0 \sigma}{4\pi R^2} , \qquad (2)$$

where I_0 is the incident intensity, and σ is the fluorescent cross section. I_0 is taken from Table I and a typical value for σ from Fig. 1. With the signal to background taken from Fig. 3 (a conservative estimate for surface impurities), the definition of the MDMF predicts that with a probe area of μm^2, in a time of one second, and with 95% confidence, the following can be detected:

2.7×10^{-4} monolayer, 5×10^3 atoms, and 40 Å-diam particle.

For a 500 $Å^2$ probe, in a time of one second, the following are typical detection limits:

5.4×10^{-3} monolayer, 250 atoms, and 15 Å-diam particle.

The assumption is made here that the particle is smaller in diameter than the probe so that reducing the probe diameter lowers the background by the square of the reduced diameter while the signal remains constant. Small probe size is a major advantage in the detection of particles smaller than the probe diameter. For an isolated particle on a very thin substrate, where the background contribution to the signal is less, even lower limits of detection can be achieved. For electron probes, the minimum detectable mass of iron in a molecule of

ferritin has been reported to be 10^{-19} g in 100 secs counting time, or 11,000 iron atoms per second at a probe current of 1.0 nA in a 60 nm-diam probe.[12] The iron K-edge fluorescent cross section for 10 keV X rays is (see Fig. 1) at least 50 times larger than for 20 keV to 100 keV electrons. So even if we ignore the better signal to background for X-ray excitation, the MDMF with X rays is less than 1/50 of that for the same electron flux. A comparison of the fluorescent analysis capabilities of X-ray and electron microprobes is given in Table II.

B. Diffraction Analysis

X rays also have some advantages over electrons when used for diffraction. Diffraction measurements provide important information such as the crystal structure, compound identification, and how the geometrical arrangements of the atoms deviate from perfect periodicity. For the same number of 10 keV X rays or electrons impinging on a metal sample, the X rays are approximately 200 times more likely than electrons to undergo a useful elastic-scattering event. Electrons are most likely to lose energy by straggling energy-loss processes adding to the unwanted background unless removed by energy-analysis spectrometers. Electrons are also more likely to undergo multiple-scattering events which complicate the interpretation of the measured diffraction pattern.[13] X-ray microprobes permit the use of thicker samples reducing the problem of defect migration to interfaces and strain relief which can be a problem in thin samples.

With the criteria expressed in Eq. 1, the MDMF by diffraction with a μm^2 X-ray probe in one second is:

10^{-2} of a monolayer, 1.6×10^3 atoms in a particle, and 28 Å-diam particle.

This is a conservative estimate as an experiment with less flux for the favorable case of a monolayer of lead deposited on the surface of a copper single crystal predicts a minimum detectable coverage of approximately 10^{-3} of a monolayer from the observed 5×10^4 signal counts s^{-1} with a signal to background of 500:1.[14] For amorphous materials, the diffuse scattering from only six monolayers of matter could be measured with a 1 μm-diam probe. Recent X-ray diffuse-scattering measurements from thin amorphous layers convinced the authors to predict that analysis of 100 Å films is feasible even at intensities 10^{-3} of those proposed for the microprobe.[15]

Among the most prominent applications of synchrotron radiation in the X-ray-energy region is the measurement of the extended X-ray absorption fine structure (EXAFS).[16] Such measurements permit the determination of the average number of near-neighboring atoms and average bond distances about a central atom whose absorption edge is scanned by changing the X-ray energy. The ability to determine the chemical environment of a particular element at low concentrations has resulted in major contributions to our understanding of the role of minor elements in matter.[17] The projected 3×10^{10} photons s^{-1} $(eV)^{-1}$ for a 500 Å-diam probe would extend the ability to make EXAFS measurements on extremely small quantities of matter and with high-spatial resolution.

A summary of the fluorescent and diffraction detectable limits of an X-ray microprobe is given in Table III.

VI. DEPTH PROFILING

The total reflection of X rays offers a means for measuring both elemental composition and phases as a function of depth from the surface. By varying the penetration depth of X rays with small glancing angles, sensitivity is increased for surface and near-surface information. Shown in Fig. 5 is the angular variation in penetration length of 17.4 keV X rays for a germanium surface.[18] For angles below about 2 mrad, only the first 25 Å contributes to the fluorescent and diffraction signal. As the grazing-incidence angle increases, the signal comes from deeper beneath the surface approaching the usual absorption penetration above 6 mrad. The development of this nondestructive X-ray-profiling technique using the highly collimated radiation from undulators would extend the advantages of X-ray fluorescent and diffraction analysis to the characterization of surfaces, overlayers, and interfaces at unprecedented low levels of detection.

VII. HEATING OF THE SAMPLE

The question arises whether excessive heating of the samples will occur from the energy in the X-ray probe. Intensities used in the detection limit calculation ranged from 10^{14} μm^{-2} to 2.5×10^{11} $(500\ Å)^2$ X rays s^{-1} and are comparable to those available in electron probes. Shown in Fig. 6 is the calculated maximum temperature rise of thin samples at the point of the beam impingement neglecting radiative heat loss.[19] A sample is thin when the absorption for the incident radiation is linearly proportional to the sample thickness. The sample is assumed to be in good thermal contact around its edge. Specimen thermal conductivities, k, and X-ray linear-absorption coefficients, μ, were chosen to span the range from good to poor thermal conductors. At the highest projected X-ray microprobe flux of 10^{14} X rays s^{-1}, good thermal conductors with low absorption coefficients would not get excessively hot. At fluxes of 10^{12} X ray s^{-1} contained in a 0.1 μm-diam probe, most samples would not be overheated. For infinitely thick samples (total absorption of the X-ray beam), the temperature rise would be from two to ten times less than given in Fig. 6. Thus, all the projected flux from undulators on low-emittance rings is useful. When appropriate, flux can be traded for improved spatial resolution. Electron microprobes deposit more energy in a smaller sample volume nearer to the surface than a similar number of X rays. Since only 10^{-3} to 10^{-4} as many X rays as electrons are required for the same MDMF, heating can be made less of a problem for X-ray microprobes.

VIII. THE NEED FOR X-RAY MICROPROBE CHARACTERIZATION OF MATERIALS

Segregation of elements and nonuniform distribution of phases in materials are the rule rather than the exception. Common interfaces in materials to which segregation occurs are surfaces, grain and precipitate boundaries, dislocations,

and surfaces formed by defects such as vacancy and interstitial configurations. Intentionally added trace elements and unintentional impurities play a major role in the physical and chemical properties of matter. Besides their effect on electrical properties, minor elements can have a major effect on both surface and mechanical properties because of their bias for segregation.[5] Segregation may extend outwardly for distances of microns from the interface or be confined to single-atomic dimensions. Microprobe characterization of segregation in materials is important to understanding their properties.

The amount of actual quantitative data on segregation of elements is rather limited; many of the observations are inferred from property changes with controlled additions of minor elements. Electron microprobes with elemental detection limits above 50×10^{-6} gg^{-1} are not sensitive enough to detect the distribution of a majority of minor elements affecting materials properties. Electron microanalysis is done mainly to identify precipitates and to study phase separation when elemental concentration differences have developed enough for detection. Much of the quantitative data on segregation to interfaces has been directed toward understanding the remarkable effect it may have on grain-boundary cohesion. Auger electron spectroscopy (AES) using electron excitation to create the signal has provided the bulk of the data from fractured surfaces. AES is a truly surface-sensitive technique detecting only the first one or two atomic layers at coverages to 0.01 of a monolayer. Because of the poor signal to background, AES is not sensitive to low concentrations. Sensitivity to the first two atomic layers precludes its use for studying interface segregation with the nominal 500 Å-diam beam end-on to the boundary. Thus fracturing in vacuum is necessary to expose the surface and preclude absorbed gases. The technique is limited to materials that can be fractured along the grain boundaries. X-ray fluorescent radiation from the K-shells of all but the lightest elements will penetrate several thousand angstroms so that detection of the grain boundary impurities can be measured with the probing beam end-on to the boundary without fracturing the specimen. The profile of the impurity distribution is inferred by deconvolution of the beam profile from the measured profile. It is very difficult with AES to be sure if the impurities are in the form of precipitates or in solution in the matrix. An X-ray microprobe could identify the two forms since diffraction analysis would identify phases and fluorescence the elements. As the chemical bonding of the segregant can change when exposed at a surface, the ability to detect impurities at an intact interface using an X-ray microprobe in the EXAFS, electron, or soft X-ray spectroscopy modes would provide information not now available.

A review of all the many obvious applications where X-ray microprobes would produce needed information for new developments in the science and technology of materials would be an enormous task. Even an order of magnitude improvement in performance over existing microprobes is sufficient justification for their funding. Gains in sensitivities of 10^3 plus the additional advantages of X rays as a probe would make it difficult to predict all the many unseen advantages. Advantages of an X-ray microprobe to a few of the large generic areas of materials science are illustrated by specific examples.

A. Crack Growth and Fracture

The catastrophic and unpredictable failure of structural components by crack initiation and propagation requires that they be greatly overdesigned compared with what is necessary to withstand the applied loads. As the basic mechanism of cracking is not well understood, expensive solutions are used: high strength is traded off for crack-resistant ductility requiring thicker members to insure reliable performance. Observations of crack initiation and propagation in thin metal foils under simple tension with transmission electron microscopy reveal the dislocation distributions associated with the plastic deformation ahead of the crack tip (Fig. 7).[20] The crack tip (at the end of the arrow) radiates dislocations in the forward direction to accommodate the high-stress levels around the crack. Quantitative information important to an understanding of the strain distributions is lost because of the necessity of using thin foils which permits buckling that relieves the elastic strain. Samples more consistent with practical situations and thick enough to preserve the elastic strain could be studied with an X-ray microprobe in diffraction gaining new information about strain distributions to test current theories of fracture.[21] In addition, the role played by impurities in fracture could be studied at concentrations orders of magnitude less than presently possible.

B. Ductile Alloys

Ordered alloys can have desirable high-temperature properties,[22] but lack of ductility greatly restricts their application. An example of such an ordered alloy lacking ductility is Ni_3Al which has superior high-temperature strength exceeding that for type 316 stainless steel and Hastelloy-X. The addition of small amounts of boron and manganese can change the cohesive energy of the grain boundaries producing a ductile material. Shown in Fig. 8, upper left, are the separated grains that resulted from hot-rolling the brittle Ni_3Al. In Fig. 8, upper right, the same material is made ductile enough to deep-draw to a 25 mm-diam cup at room temperature after minor alloying additions. The curve in the lower part of Fig. 8 shows the dramatic change in the tensile elongation with the addition of boron. Auger electron spectroscopy was used to show that boron is segregated to the grain boundaries, but the chemical form of the boron could not be determined.[23] An X-ray microprobe with orders of magnitude better signal to noise would provide both diffraction and elemental analysis producing information on chemical bonding at interfaces without having to fracture the surfaces.

C. Creep

A mode of deformation of crystalline materials held at high temperatures under low stresses is grain-boundary creep. An example of the failure of a Ni-20 wt % Cr-alloy by this process is shown in Fig. 9. Grain-boundary creep followed by crack initiation and propagation leads to rupture of the sample. Use of interface-active solutes is a means of changing the rate of this diffusion-controlled creep. The addition of 0.11 wt % Zr to a Ni-Cr alloy is shown in Fig. 10 to have a major effect on improving the creep-rupture performance by extending the service life and reducing the elongation while increasing

the load-carrying capacity.[24] X-Ray microprobe measurements of the elemental segregation to the grain boundaries, grain boundary diffusivity, and the strain and deformation present at the boundaries would provide new information towards understanding and controlling this phenomenon.

D. Ceramics

The brittleness of ceramic materials prevents their desirable high-temperature strength, wear, and corrosion resistance from being widely used in structural applications. Design criteria are uncertain since crack initiation and propagation are poorly understood. Fracturing occurs over a wide range of stresses and is influenced by poorly understood impurities at interfaces. Sintering ceramics to high density improves their resistance to fracturing apparently by reducing the voids which act to initiate cracks along the grain boundaries.[25] Among the methods used to achieve high-sintering densities and to increase toughness are the additions of small amounts of other elements which segregate to grain boundaries. An example of the effect of magnesium on the sintered density of alumina is the development by the General Electric Company of optically translucent alumina (Lucalox) for use in high-pressure sodium lamps. Though several studies have shown that the magnesium segregates to the grain boundaries, from the standpoint of the chemistry that occurs at the boundary, the effect is poorly understood.[26] Second phase additions are also used to control grain boundary fracture in the development of tougher ceramics. More ductile metals or ceramics placed in the grain boundaries will absorb some of the energy by plastic deformation. An example in zirconia-toughened alumina is shown in Fig. 11. The darker particles in this transmission electron micrograph are zirconia which undergo a phase transformation under stress absorbing energy from the crack. Thus more stress is required to propagate the crack. X-ray microprobe measurement of the strain distributions in the grains adjacent to the crack, of second phases by diffraction, and of the elemental segregation by fluorescence would provide new information on which to base our understanding for improved crack-resistant ceramics.

E. Diffusion

The rate of diffusion of elements is important whenever dissimilar materials are in contact. Diffusion controls the characteristics of mass transport which includes the rate at which chemical equilibrium is reached, the rate of growth and dissolution of precipitates, corrosion rates, and rates of transformation. Since most materials consist of more than one element, knowledge of the lattice and short-circuiting paths of diffusion is key information to the design of new materials. Diffusion rates are necessary to understand the thermodynamics of phase equilibria, the kinetics of transformations, and in particular the way materials undergo radiation damage such as from ion implantation and fusion or fission reactors. An X-ray microprobe detecting concentrations at 10^{-9} gg^{-1} levels with fractional μm resolutions would be extremely useful for obtaining diffusion information. In short-circuit diffusion where data are difficult to obtain, radioactive tracers are often used. An example is shown in Fig. 12 where radioactive Ni63 is used to obtain an autoradiographic image of nickel diffusion into a copper grain boundary.[27]

Densitometer measurements of the exposed film were made with a 6.3 × 6.3 μm^2 slit. An X-ray microprobe would have the elemental sensitivity to directly determine quantitatively the concentration gradients for the diffusion of unlike elements.

Preferential corrosion along grain boundaries is common in stainless steels, and nickel-, chromium-, and aluminum-base alloys in aqueous environments. Trace element segregation to the boundaries is associated with a sensitization mechanism that may have a large effect on intergranular corrosion. A lack of chemical information about the boundary leaves the process poorly understood.

F. Electronics

The science and technology of designing and fabricating high-performance and reliable integrated circuits and microchips are dependent in a large measure on the control of certain impurities and trace-element additions which are generally below the detectable limits of electron probes. Miniaturization in integrated-circuit technology and increasing circuit densities on microchips with spacing of 1 µm or less have pushed the requirements for chemical, structural, and elemental information to levels below what can presently be detected in such small dimensions. A silicon chip on an electronic circuit board is shown in Fig. 13. Literally millions of electrical contacts are made and reliability depends on each performing satisfactorily. The failure of micrometer-sized connections and circuits occurs from aging mechanisms such as grain growth, interdiffusion, surface crystallization, and crack propagation. An accelerated understanding of this degradation requires microcharacterization at levels below those presently obtainable. Because of the part per billion detection capabilities with submicron resolutions, X-ray probes will have wide application in the electronics industry.

G. Radiation Effects

Structural materials are subjected to high doses of energetic radiation in existing fission and planned fusion reactors. Important changes in their physical properties include swelling, creep, and embrittlement. Another form of irradiation is ion implantation to control surface and near-surface properties. Common to both processes are the large number of point defects produced by direct displacement of the atoms in the material and the alterations of the composition by transmutations or implantation of different elements. The high flux of vacancies and interstitials leads to enhanced diffusion which may induce segregation and precipitation at interfaces or void formation by vacancy collection. To improve radiation resistance, efforts are made to promote the removal of vacancies and interstitials by recombination or to prevent the agglomeration of like defects.[28] Shown in Fig. 14(a) are the voids generated by irradiation of an unmodified stainless steel leading to large swelling of the alloy. The additions of 0.2 wt % titanium to the steel dramatically reduces the swelling as shown in Fig. 14(b). Grain boundaries, dislocations, precipitates, and substitutional elements can act as sinks for the point defects and/or promote their recombination. Electron microprobe and transmission electron microscopy are

extensively used for microcharacterization of radiation damage and much remains to be done to understand this complex phenomenon. An X-ray microprobe will bring needed new information to this materials problem with 10^{-3} or lower elemental detection limits, diffraction information about strain and precipitation, and with chemical bonding insights obtained through EXAFS and other spectroscopies.

ACKNOWLEDGMENTS: To G. E. Ice for useful calculations and comments on the manuscript, to H. L. Yakel for his corrections to the manuscript, and to many of my colleagues who were willing to share their research problems with me and to provide figures.

REFERENCES

[1]Cosslett, V. E., A. Engström, and H. H. Pattee, Jr., eds. 1957. X-Ray Microscopy and Microradiography, New York: Academic Press, Inc.

[2]Zaluzec, N. J. 1979. Quantitative x-ray microanalysis: instrumental consideration and applications to materials science. Chapter 4, pp. 121–167 in Introduction to Analytical Electron Microscopy, J. J. Hern, J. I. Goldstein, and D. C. Joy, eds. New York: Plenum Press.

[3]Kriege, O. H. and J. Y. Marks 1976. Nonuniform distribution (both micro and macro) of trace elements in high-temperature alloys. Pp. 1017–1022 in National Bureau of Standards Special Publication 422, Accuracy in Trace Analysis: Sampling, Sample Handling, Analysis, Vol. II, P. D. LaFleur, ed. Washington, D.C.: U. S. Government Printing Office.

[4]Davis, C. M. 1976. Trace element analysis of nickel and nickel-base alloys — a review of current methods. Pp. 1005–1016 in National Bureau of Standards Special Publication 422, Accuracy in Trace Analysis: Sampling, Sample Handling, Analysis, Vol. II, P. D. LaFleur, ed. Washington, D.C.: U. S. Government Printing Office.

[5]Hondros, E. D. and M. P. Seah 1977. Segregation to Interfaces. International Metals Review 22:262–301.

[6]Currie, L. A. 1968. Limits for qualitative detections and quantitative determination. Anal. Chem. 40:586–593.

[7]Sparks, C. J., Jr. 1980. X-ray fluorescence microprobe for chemical analysis. Chapter 14, pp. 459–512 in Synchrotron Radiation Research, H. Winick and S. Doniach, eds. New York: Plenum Press.

[8]Slatkin, D. N., A. L. Hanson, K. W. Jones, H. W. Kramer, and J. B. Warren 1984. Damage to air-dried human blood cells and tissue sections by synchrotron radiation. Brookhaven National Laboratory Report BNL-34555.

[9]Howells, M. R. and J. B. Hastings 1983. Design considerations for an x-ray microprobe. Nucl. Instr. and Meth. 208:379–386.

[10]Ice, G. E. and C. J. Sparks, Jr. 1984. Focusing optics for a synchrotron x-radiation microprobe. Nucl. Instr. and Meth. In press.

[11]Goldstein, J. I. 1979. Principles of thin film x-ray microanalysis. Chapter 3, pp. 83–120 in Introduction to Analytical Electron Microscopy, J. J. Hern, J. I. Goldstein, and D. C. Joy, eds. New York: Plenum Press.

[12]Shuman, H. and A. P. Somlyo 1976. Electron probe x-ray analysis of single ferritin molecules. Proc. Nat. Acad. Sci. USA 73(4):1193–1195.

[13]Cowley, J. W. 1975. Diffraction Physics, New York: American Elsevier.

[14]Marra, W. C., P. H. Fuoss, and P. E. Eisenberger 1982. X-ray diffraction studies: melting of Pb monolayers on Cu(110) surfaces. Phys. Rev. Lett. 49(16):1169–1172.

REFERENCES (cont.)

[15]Fischer-Colbrie, A., P. H. Fuoss, M. Marcus, and A. Bienenstock 1983. X-ray scattering study on thin amorphous films. Pp. VII—140,141 in SSRL Report 83/01, K. Cantwell, ed.

[16]Winick, H. and S. Doniach, eds. 1980. Chapters 10—13 in Synchrotron Radiation Research, New York: Plenum Press.

[17]Bianconi, A., L. Incoccia, and S. Stupcich, eds. 1983. Proceedings of Second International Conference on EXAFS and Near-Edge Structure, New York: Springer-Verlag.

[18]Becker, R. S., J. A. Golovchenko, and J. R. Patel 1983. X-ray evanescent-wave absorption and emission. Phys. Rev. Lett. 50(3):153—156.

[19]Hobbs, L. W. 1979. Radiation effects in analysis of inorganic specimens by TEM. Chapter 17, pp. 437—480 in Introduction to Analytical Electron Microscopy, J. J. Hern, J. I. Goldstein, and D. C. Joy, eds. New York: Plenum Press.

[20]Kobayaski, S. and S. M. Ohr 1981. In situ observations of the formation of plastic zone ahead of a crack tip in copper. Scripta Metallurgica 15:343—348.

[21]Ohr, S. M. and S.-J. Chang 1982. Dislocation-free zone model of fracture: comparison with experiments. J. Appl. Phys. 53(8):5645—5651.

[22]Stoloff, N. S. and R. G. Davies 1966. The mechanical properties of ordered alloys, Vol. 13 in Progress in Metal Science, B. Chalmers and W. Hume-Rothery, eds., New York: Pergamon Press.

[23]Liu, C. T., C. L. White, C. C. Koch, and E. H. Lee 1983(7). Preparation of ductile nickel aluminides for high temperature use. Pp. 32—41 in Proceedings of the Symposium on High Temperature Materials Chemistry-II, Z. A. Munir and D. Cubicciotti, eds. Pennington, N. J.: The Electrochemical Society, Inc.

[24]Schneibel, J. H., C. L. White, and M. H. Yoo 1984. On the improvement of creep strength and ductility of Ni-20% Cr by small zirconium additions. Submitted for publication to Metall. Trans.

[25]Rice, R. W. 1977. Microstructural dependence of mechanical behavior of ceramics. Pp. 199—381 in Treatise on Materials Science and Technology, Vol. II, Properties and Microstructure, New York: Academic Press.

[26]Taylor, R. I., J. P. Coad, and A. E. Hughes 1976. Grain-boundary segregation in MgO-doped Al_2O_3. J. Am. Ceram. Soc. 59(7,8):374—375.

[27]Renouf, T. J. 1970. The measurement of grain boundary diffusion by the method of autoradiography. Phil. Mag. 22(176):359—375.

[28]Mansur, L. K. and E. E. Bloom 1982. Radiation effects in reactor structure alloys. J. of Metals 34(10):23—31.

TABLE I. Comparison of X-ray microprobe intensities from 6 GeV ring.

	14 keV X-rays 2.5 GeV, 500 mA wiggler	14 keV X-rays 6 GeV, 200 mA undulator	100 keV e^- Electron microprobe field emission[a]
Brightness Photons or e^-/s mm^2 $mrad^2$	10^{16}[b]	2×10^{19}[b,c]	3×10^{19}
	$\frac{5 \times 10^{12}}{10\ \mu m^2\ s\ 280\ eV}$	$\frac{2 \times 10^{15}}{10\ \mu m^2\ s\ 10\ eV}$	
	$\frac{5 \times 10^{11}}{\mu m^2\ s\ 280\ eV}$	$\frac{1 \times 10^{14}}{\mu m^2\ s\ 10\ eV}$	$\frac{6 \times 10^{13}}{\mu m^2\ s\ eV}$[d]
Intensity P or e^-/Area sec	$\frac{1 \times 10^{9}}{500\ Å^2\ s\ 280\ eV}$	$\frac{3 \times 10^{11}}{500\ Å^2\ s\ 10\ eV}$	$\frac{6 \times 10^{11}}{500\ Å\ s\ eV}$
			$\frac{6 \times 10^{9}}{30\ Å^2\ s\ eV}$
			$\frac{10^{7}}{4\ Å^2\ s\ eV}$

[a] Zaluzec, N. J. 1979. Quantitative x-ray microanalysis: instrumental considerations and applications to materials science. Chapter 4, pp. 121–67 in Introduction to Analytical Electron Microscopy, J. J. Hern, J. I. Goldstein, and D. C. Joy, eds. New York: Plenum Press.

[b] National Synchrotron Light Source, Planned Evolution of NSLS, October 1983.

[c] Stanford Synchrotron Radiation Laboratory, SSRL Report 83/01.

[d] LaB_6 electron source.

TABLE II. Comparison of the characteristics of the proposed X-ray microprobe with those of the most advanced electron microprobes for fluorescent chemical analysis.

Characteristics	X rays	Electrons
Minimum detectable mass fraction s^{-1} for 1 μm-diam probe	0.01 ppm	50 ppm
Minimum detectable mass s^{-1} for 500 Å probe	250 atoms	10,000 atoms
Minimum spatial resolution (samples > 1 μm thick)	~500 Å	10^3 to 10^4 Å
Minimum spatial resolution (samples 100 Å to 2000 Å thick)	~500 Å	10 to 500 Å
Number of electrons and X rays for the same MDMF	1	10^3
Number of energy units deposited in thick targets for same MDMF	1	10^3 to 10^4
Operating atmosphere	air, gas water, vapors	vacuum
Relative signal to background (contrast)	10^4	1
Accuracy for quantitative analysis: similar standards	~1%	~10%
Accuracy for quantitative analysis: pure element standards	~5%	>10%
Relative fluorescent cross section	10 to 200	1
Relative thick-target fluorescent yields	10 to 150	1
Charge collection on electrically insulating samples	negligible	must be coated with conducting film

TABLE III. Detection limits for an X-ray microprobe based on radiation from an undulator on a 6 GeV low emittance storage ring.

Distributions of the elements	Probe size	Detection limits by fluorescent analysis	Detection limits by diffraction analysis
Homogeneous	1 μm-diam	10^{-8} gg^{-1} s^{-1}	$<10^{-4}$ gg^{-1} s^{-1}
Embedded planer interfaces	1 μm- to 500 Å-diam	5×10^{-5} monolayers s^{-1} 5×10^{-3} monolayers s^{-1} in presence of 0.1 gg^{-1}	< monolayer
Surface atoms or particles	1 μm-diam	2.7×10^{-4} monolayers s^{-1} 5×10^{3} atoms s^{-1} 40 Å-diam particle s^{-1}	Crystalline 10^{-2} monolayers s^{-1} 1.6×10^{3} atoms s^{-1} 28 Å-diam particle s^{-1} Amorphous 6 monolayers s^{-1}
	500 Å-diam	5.4×10^{-3} monolayers s^{-1} 250 atoms s^{-1} 15 Å-diam particle s^{-1}	

FIGURE CAPTIONS

Fig. 1 Fluorescence cross sections for the elements when excited by X rays, protons ($^1H^+$), and electrons (e) of varying energies (after Sparks[7]).

Fig. 2 Thick-target fluorescence yields of pure elements for X rays, protons, and electrons of varying energies (after Sparks[7]).

Fig. 3 Comparison of the fluorescent signal-to-background ratio for various excitation radiations at a concentration of 10^{-6} gg^{-1} for an X-ray fluorescent radiation detection system with an energy resolution of the natural linewidth (after Sparks[7]).

Fig. 4 Calculated fluorescent intensity profile for an X-ray microprobe scan over a grain boundary containing a monolayer of titanium when the iron matrix contains 0.1 wt % titanium.

Fig. 5 Penetration depth of 17.4 keV X rays into germanium varies as a function of grazing incidence angle, α, to provide for nondestructive profiling of chemical information (after Becker et al[18]).

Fig. 6 Temperature rise from a 1 μm-diam X-ray beam impinging on a thin 10 mm-diam sample with side cooling. k/μ is the thermal conductivity in W/m•K divided by the X-ray linear absorption coefficient in m^{-1}. The k/μ values for various elements and materials are shown.

Fig. 7 Transmission electron micrograph of a shear crack with the dislocation network forming the plastic zone ahead of the crack (after Kobayaski and Ohr[20]).

Fig. 8 Brittle materials such as Ni_3Al shown with its grains separated in the upper left can be made ductile as illustrated by the cup (25 mm-diam) deep-drawn at room temperature. The lower curve shows the dramatic effect of adding boron to improve the ductility. Little is known about the chemical effect boron has on increasing the cohesion of the grain boundaries (courtesy of C. T. Liu, Oak Ridge National Laboratory).

Fig. 9 Failure of a Ni-20 wt % Cr alloy at 800°C by grain boundary fracture (courtesy of J. H. Schneibel, Oak Ridge National Laboratory).

Fig. 10 Segregation of minor concentrations of elements can effect the mechanical properties of materials through grain boundary modifications (after J. H. Schneibel et al[24]).

Fig. 11 Grain boundary cracking in ceramics is a major limitation to their application as structural members. Additions of 20 vol % ZrO_2 (the darker particles in this transmission electron micrograph) to Al_2O_3 improves the resistance to cracking (courtesy of P. F. Becher, Oak Ridge National Laboratory).

FIGURE CAPTIONS (cont.)

Fig. 12 An autoradiographic image of Ni_{63} tracer diffusion into a copper grain boundary. Diffusion along the boundary occurres at a faster rate than through the grain (after T. J. Renouf[27]).

Fig. 13 Advancements in minaturization and reliability of electron circuit boards and silicon microchips as shown here require nondestructive microcharacterization at submicron resolutions and below the detectable limits of electron microprobes.

Fig. 14 (a) Stainless steel of composition Fe-13 wt % Cr-15 wt % Ni irradiated with 4 meV Ni^{++}_{ions} to a dose of 70 displacements per atom at 675°C. The formation of many voids caused the alloy to swell. (b) Same composition and irradiation as in (a) except for 0.2 wt % Ti addition; the swelling was reduced dramatically (courtesy of Eal Lee, Oak Ridge National Laboratory).

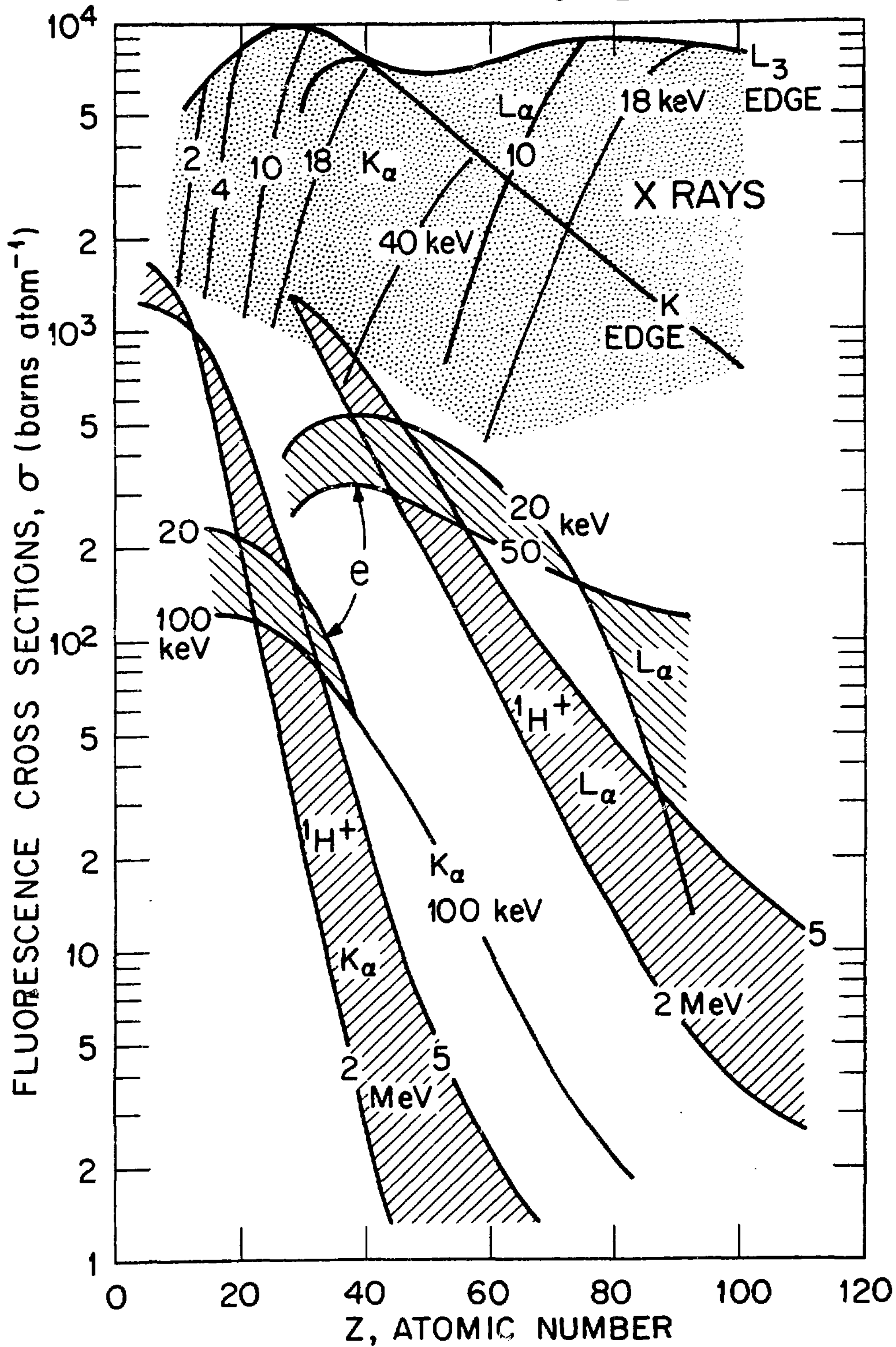
ORNL-DWG 78-17707R
FLUORESCENCE CROSS SECTIONS, σ (barns atom⁻¹)
Z, ATOMIC NUMBER
X RAYS
L3 EDGE
K EDGE
18 keV
40 keV
20 keV
50
100 keV
2 MeV
5
e
Kα
Lα
¹H⁺

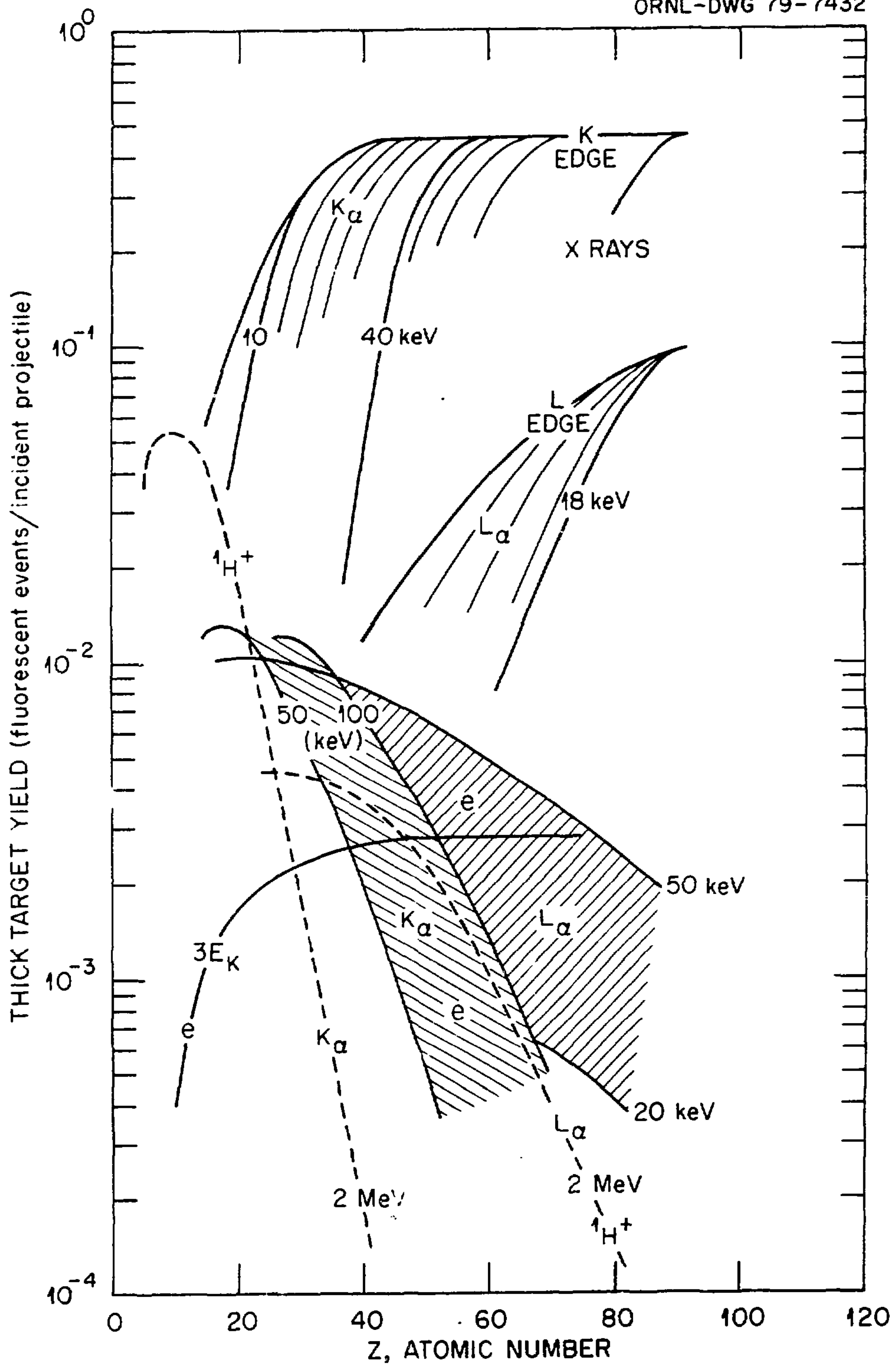

ORNL-DWG 79-7432
THICK TARGET YIELD (fluorescent events/incident projectile)
10^{0}
10^{-1}
10^{-2}
10^{-3}
10^{-4}
Z, ATOMIC NUMBER
0
20
40
60
80
100
120
K EDGE
X RAYS
K_α
10
40 keV
L EDGE
L_α
18 keV
$^1H^+$
50 100 (keV)
e
50 keV
$3E_K$
20 keV
2 MeV

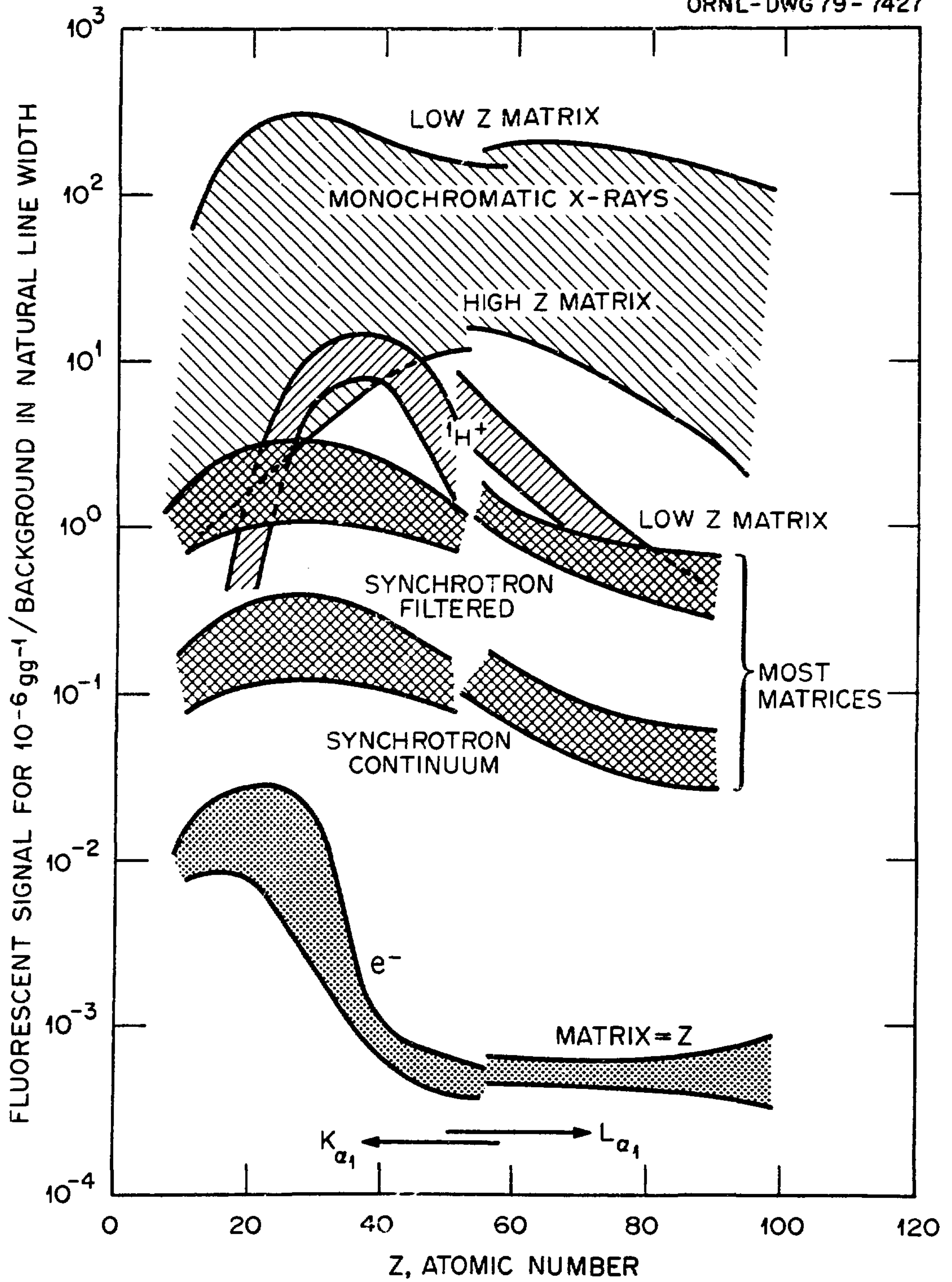
ORNL-DWG 79-7427
LOW Z MATRIX
MONOCHROMATIC X-RAYS
HIGH Z MATRIX
$^1H^+$
LOW Z MATRIX
SYNCHROTRON
FILTERED
MOST
MATRICES
SYNCHROTRON
CONTINUUM
e⁻
MATRIX = Z
K_{α_1}
L_{α_1}
FLUORESCENT SIGNAL FOR 10^{-6} gg^{-1}/BACKGROUND IN NATURAL LINE WIDTH
Z, ATOMIC NUMBER
10^3
10^2
10^1
10^0
10^{-1}
10^{-2}
10^{-3}
10^{-4}
0
20
40
60
80
100
120

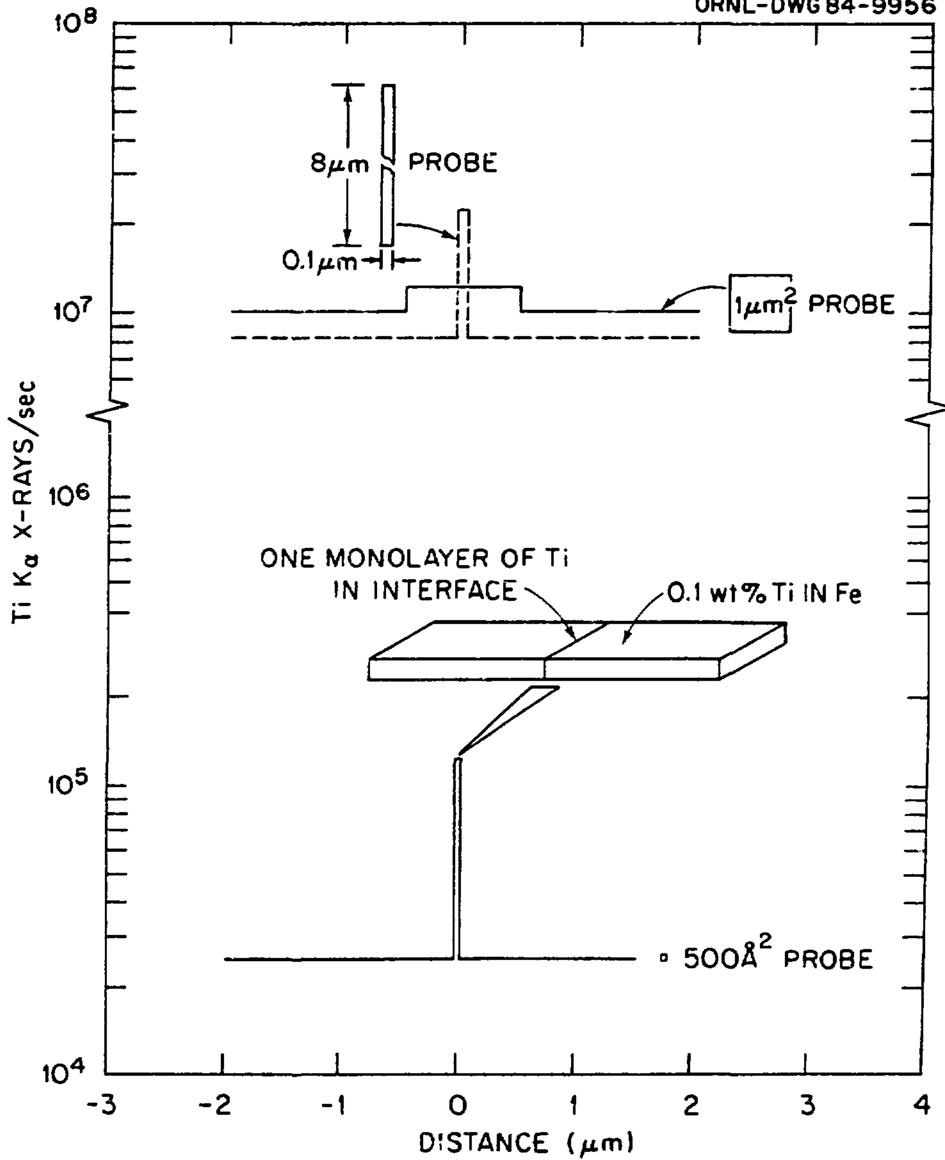
ORNL-DWG 84-9956
8μm
PROBE
0.1μm
1μm² PROBE
ONE MONOLAYER OF Ti
IN INTERFACE
0.1 wt% Ti IN Fe
500Å² PROBE
Ti Kα X-RAYS/sec
DISTANCE (μm)
10⁸
10⁷
10⁶
10⁵
10⁴
-3
-2
-1
0
1
2
3
4

ORNL-DWG 84-9955

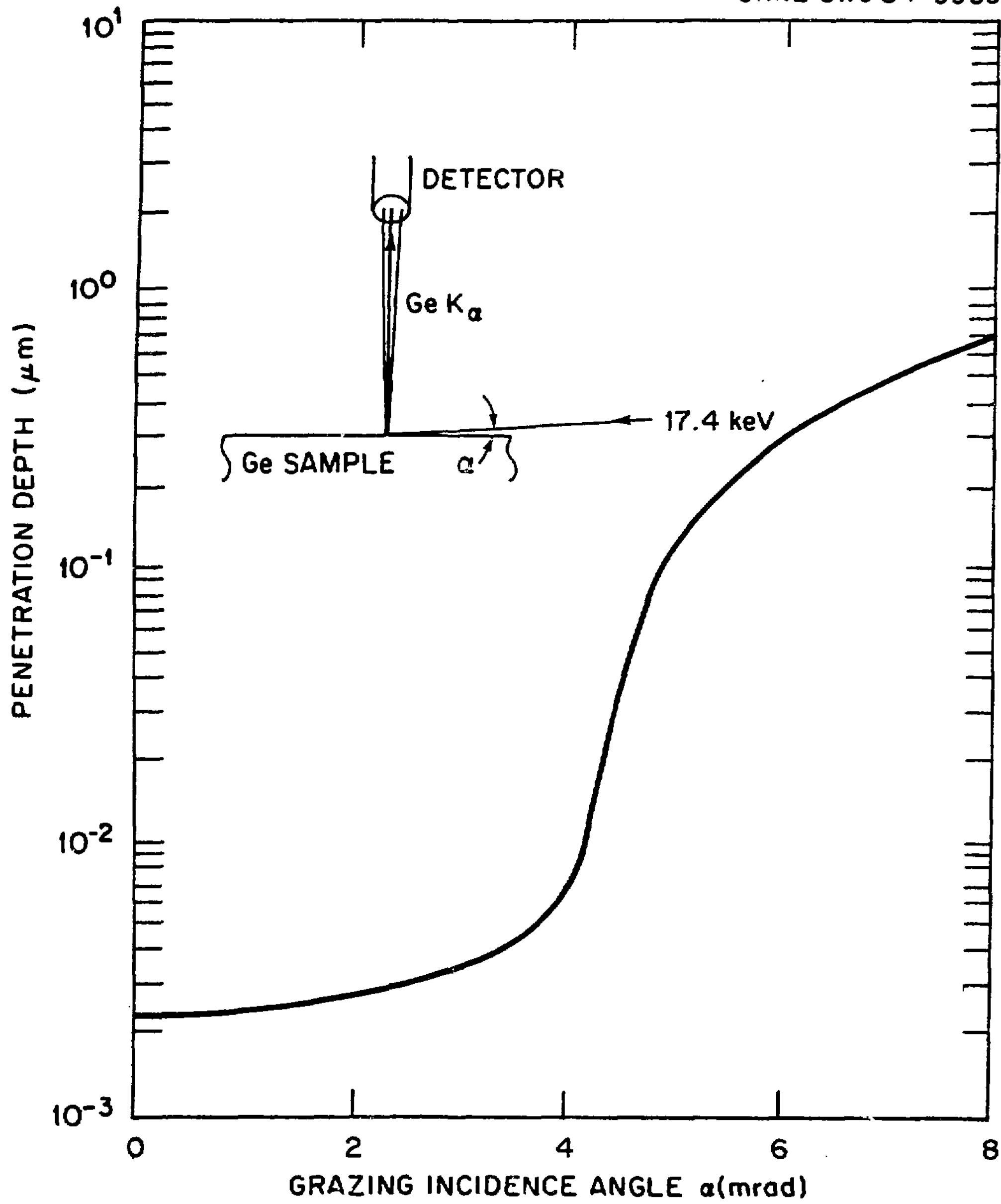

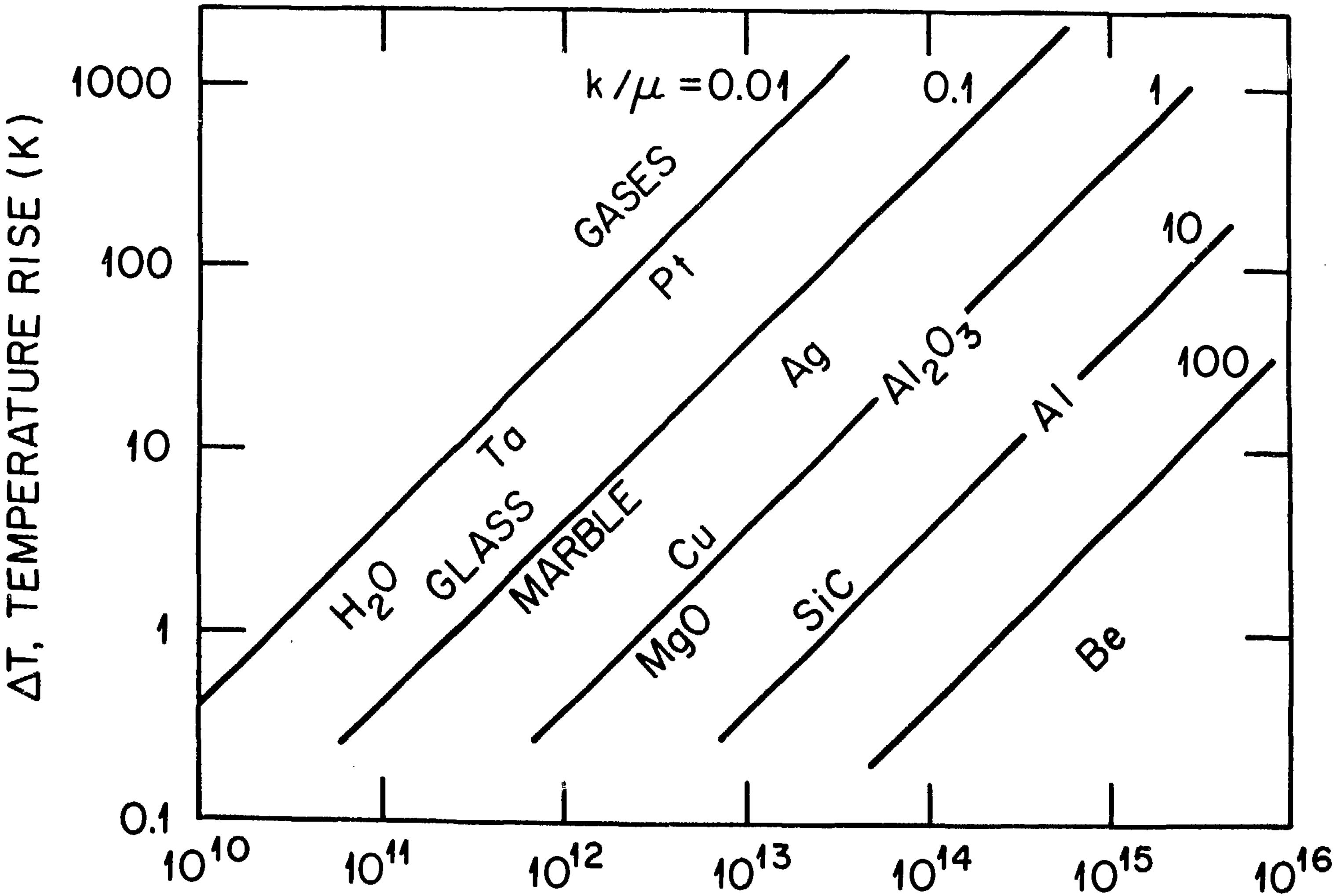
ORNL-DWG 84-10848
k/μ = 0.01
0.1
1
10
100
GASES
Pt
Ta
H2O
GLASS
MARBLE
Ag
Cu
MgO
Al2O3
Al
SiC
Be
1000
100
10
1
0.1
10^10
10^11
10^12
10^13
10^14
10^15
10^16
ΔT, TEMPERATURE RISE (K)
INCIDENT BEAM FLUX (15 keV X-RAYS s^-1)

g=[$\bar{1}\bar{1}$1]
(123)
2 μm

NICKEL ALUMINIDES BASED ON Ni_3Al CAN BE MADE DUCTILE BY MICROALLOYING

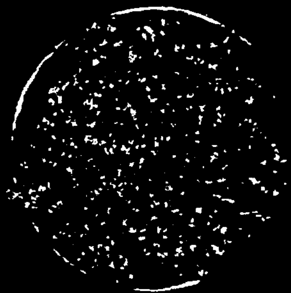

UNMODIFIED Ni_3Al

Ni_3Al DOPED WITH B AND Mn

- THE ALUMINIDES ARE MUCH STRONGER THAN STAINLESS STEELS AND SUPERALLOYS AT ELEVATED TEMPERATURES

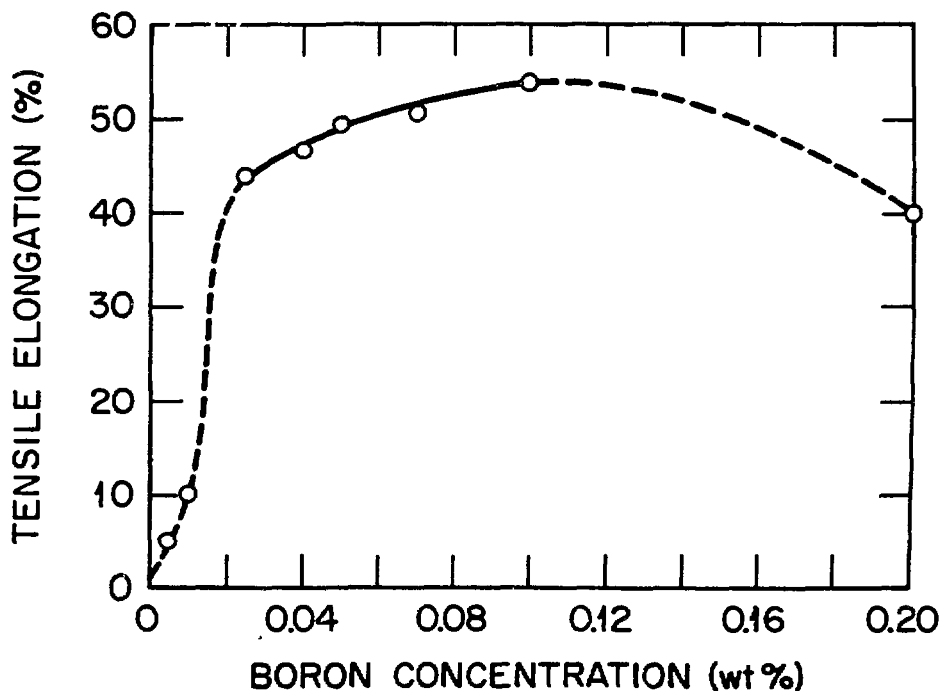

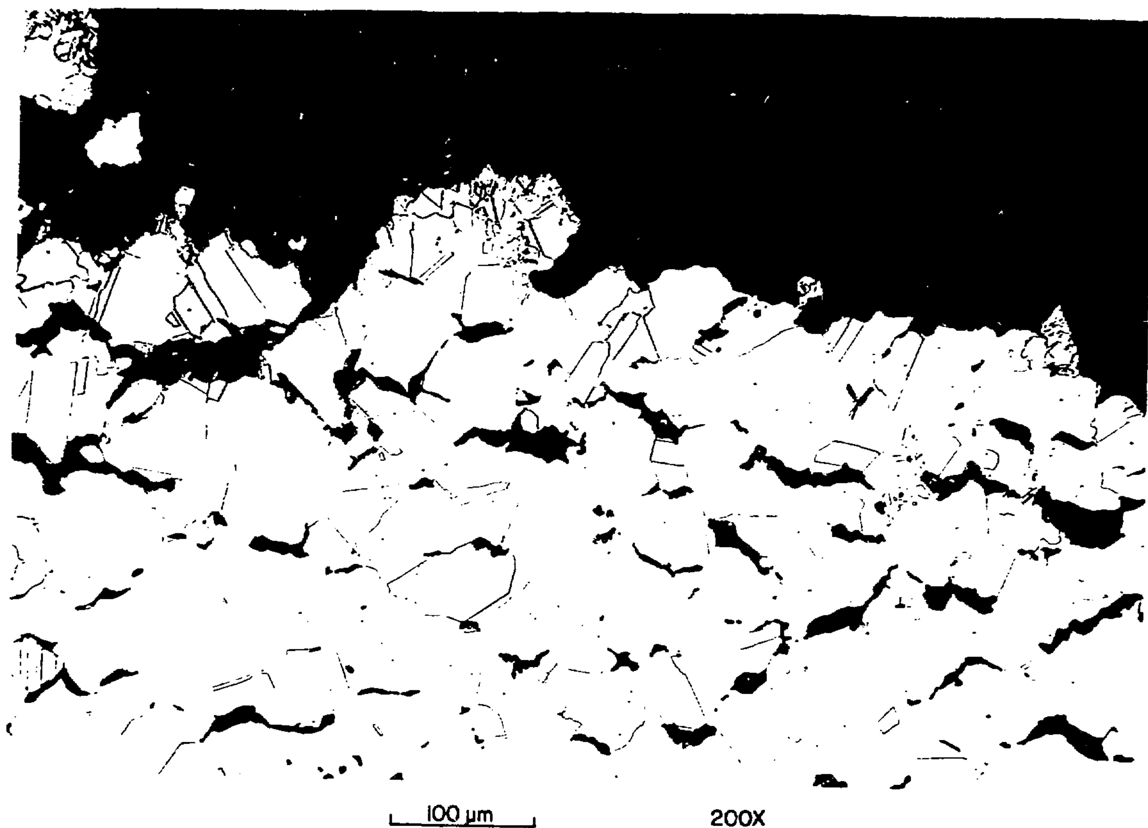
100 μm
200X

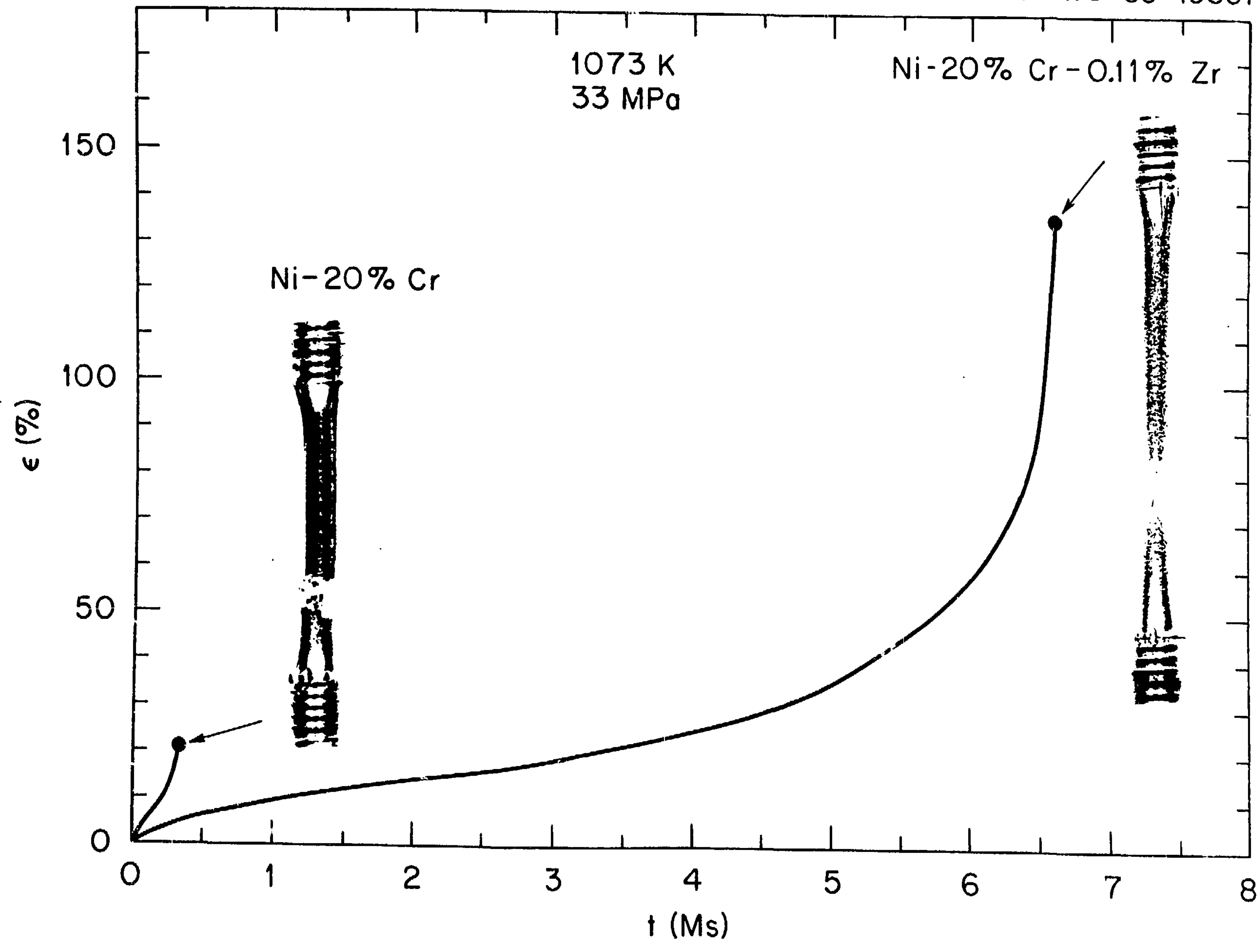
ORNL-DWG 83-19851
1073 K
33 MPa
Ni-20% Cr-0.11% Zr
Ni-20% Cr
ε (%)
t (Ms)
0
50
100
150
0
1
2
3
4
5
6
7
8

Mag = (2.0×57,000)

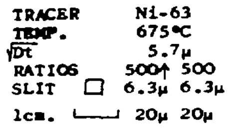

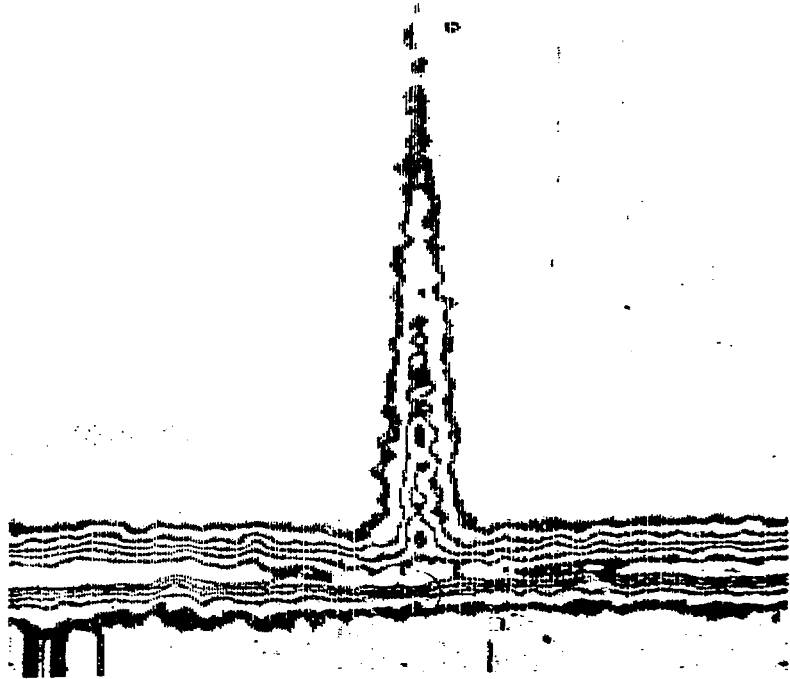

(a)

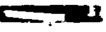

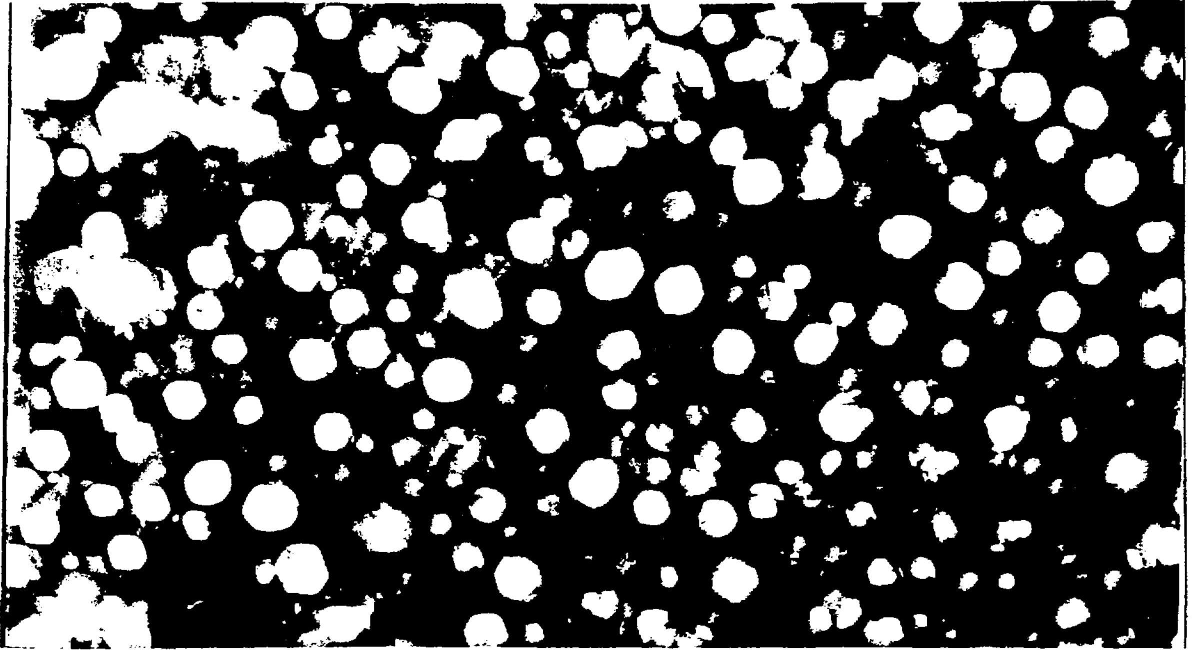

a.

b.